Acta Crystallographica Section C
Crystal Structure Communications
ISSN 0108-2701

Supramolecular study, Hirshfeld analysis and theoretical study of 6-methoxyquinoline *N*-oxide dihydrate

Rodolfo Moreno-Fuquen,[a]* Geraldine Hernandez,[a] Alan R. Kennedy[b] and Catriona A. Morrison[b]

[a]Departamento de Química, Facultad de Ciencias, Universidad del Valle, Apartado 25360, Santiago de Cali, Colombia, and [b]WestCHEM, Department of Pure and Applied Chemistry, University of Strathclyde, 295 Cathedral Street, Glasgow G1 1XL, Scotland
Correspondence e-mail: rodimo26@yahoo.es

Received 17 October 2012
Accepted 1 May 2013

In the crystal structure of 6-methoxyquinoline *N*-oxide dihydrate, $C_{10}H_9NO_2{\cdot}2H_2O$, (I), the presence of two-dimensional water networks is analysed. The water molecules form unusual water channels, as well as two intersecting mutually perpendicular columns. In one of these channels, the O atom of the *N*-oxide group acts as a bridge between the water molecules. The other channel is formed exclusively by water molecules. Confirmation of the molecular packing was performed through the analysis of Hirshfeld surfaces, and (I) is compared with other similar isoquinoline systems. Calculations of bond lengths and angles by the Hartree–Fock method or by density functional theory B3LYP, both with 6-311++G(d,p) basis sets, are reported, together with the results of additional IR, UV–Vis and theoretical studies.

Comment

Aromatic nitrogen heterocycles are widely used as, amongst other things, versatile chelating agents [see, for example, Katakura & Koide (2006)], precursors to pesticides (Kaiser *et al.*, 1996) and bioactive materials (Polshettiwar & Varma, 2008). It is thought that the presence of a quinoline ring is the key factor responsible for imparting a wide range of medicinal properties (Somvanshi *et al.*, 2008), reflected in the behaviour of quinoline derivatives as antibacterial agents (Towers *et al.*, 1981), antifungal agents (Biavatti *et al.*, 2002), cytotoxic compounds (Sui *et al.*, 1998) and drugs (Campbell *et al.*, 1988). The formation of such compounds with *N*-oxide groups has also been driven by their important pharmacological applications (Ballabio *et al.*, 1992) and has additionally attracted the interest of those developing the field of crystal engineering and the science of organic materials (Desiraju, 1989).

In hydrated crystal systems, it is interesting to analyse the presence and role of water molecules in specific structures. The formation of one- or two-dimensional water chains in a crystal structure can define the behaviour and properties of that system (Cukierman, 2000). Indeed, a large number of biological processes appear to depend on the behaviour of these water chains (Jude *et al.*, 2002). For example, proton translocation processes through membranes are assisted by chains of water molecules functioning as 'proton wires' (Tieleman *et al.*, 2001).

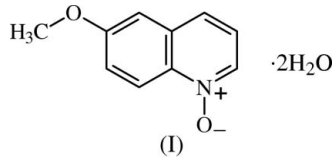

(I)

These two themes of *N*-oxide-bearing quinolines and hydrated solid-state structures have been combined by examining the structure of 6-methoxyquinoline *N*-oxide (MQNO) as its dihydrate, (I). This is part of our ongoing investigation of the structural properties of the isoquinoline matrix and extends earlier work from our research group that reported the structure of the biomolecule 2-amino-3-(*N*-oxypyridin-4-ylsulfanyl)propionic acid in its dihydrate phase, and which showed that the molecules of the compound are stabilized by the formation of one-dimensional water chains (Moreno-Fuquen *et al.*, 2010). Herein, we describe the crystal structure of (I) and provide spectroscopic (IR and UV–Vis) analysis. Additional theoretical studies and an analysis of Hirshfeld surfaces were also carried out. It is important to consider the presence of water molecules and their interactions within supramolecular synthons through hydrogen bonds and other intermolecular interaction patterns (Desiraju, 1996). Thus, this last analysis was performed to confirm the molecular packing of the system, by examining the behaviour of intermolecular interactions on these surfaces (McKinnon *et al.*, 2004).

Some of the derivatives of the isoquinoline matrix, the 6-methoxyquinoline *N*-oxide–hydroquinone (2/1) cocrystal (MQNOHQ; Moreno-Fuquen *et al.*, 2007), 2,4-dichloro-6-

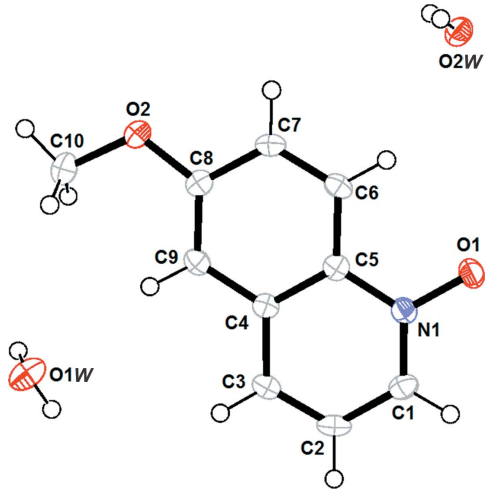

Figure 1
A view of the components of (I), showing the atom-numbering scheme. Displacement ellipsoids are drawn at the 50% probability level.

 doi:10.1107/S0108270113011979

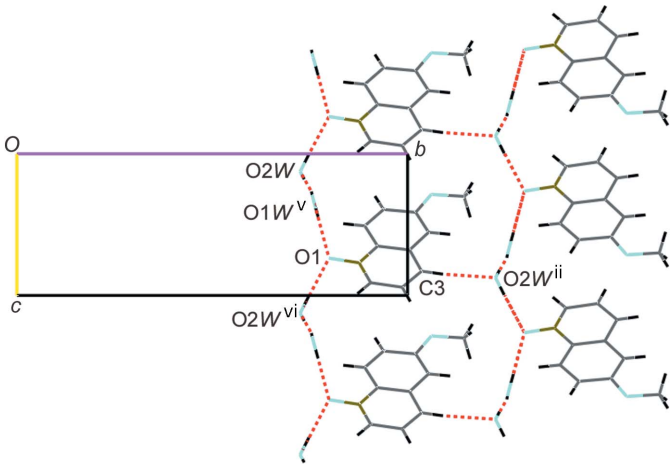

Figure 2
Part of the crystal structure of (I), showing the formation of channels of water molecules along [001]. [Symmetry codes: (ii) $-x+1, y+\frac{1}{2}, -z+1$; (v) $-x+1, y-\frac{1}{2}, -z+1$; (vi) $x, y, z+1$.]

methoxyquinoline (Subashini *et al.*, 2009) and other 6-methoxyquinoline derivative structures (Chambers *et al.*, 2004), are available as reference systems with which to compare the structural characteristics of (I). The molecular structure of (I) is shown in Fig. 1. Coplanarity between the quinoline ring and the methoxy group (C5—O2—C10) is observed in (I). This same coplanarity is observed for 2,4-dichloro-6-methoxyquinoline, and only a small deviation from coplanarity is seen in MQNOHQ [dihedral angle = 3.1 (1)°]. Other bond lengths and angles of the isoquinoline ring of (I) agree with literature values (Allen *et al.*, 1987).

The inclusion of water molecules in the quinoline structure can potentially result in the formation of intermolecular hydrogen bonds, which allows a more stable crystal structure. In the anhydrous 6-methoxyquinoline *N*-oxide system, wherein intermolecular interactions should be relatively weak, this behaviour should not be observed. The presence of water molecules in the quinolinic structure of (I) allows the formation of relatively strong O—H···O hydrogen bonds, thereby stabilizing the crystal structure (Table 1; Nardelli, 1995).

Achiral (I) crystallizes in the monoclinic Sohncke space group $P2_1$, possibly motivated by a chiral environment imposed by the lattice (Sakamoto, 2004) or by the formation of chains of hydrogen-bonding character (Leiserowitz & Weinstein, 1975). Compound (I) should display relatively strong hydrogen bonds between the methoxyquinoline ring and the water molecules. Indeed, (I) exhibits two sets of strong water–quinoline O—H···O and two sets of strong water–water O—H···O interactions (see Table 1 for full details). Weak C—H···O interactions (Table 1) complement the strong hydrogen bonds.

A supramolecular analysis of (I) reveals, in the first substructure, the presence of channels formed by water molecules and atom O1 of the N—O group. Indeed, atom O1 acts simultaneously as a hydrogen-bond acceptor from atom O1*W*$(-x+1, y-\frac{1}{2}, -z+1)$ and from atom O2*W*$(x, y, z+1)$. Atom O2*W* is linked to another O1*W* atom and this latter atom is linked to the next O1 atom of the *N*-oxide group, and so on. Thus, these channels are characterized by the presence of three molecules of water followed by an O atom of the *N*-oxide group, and this latter atom acts as a bridge between the water molecules running along [001] (Fig. 2). Also in Fig. 2, one can see that (I) interacts with a second water channel through the weak C3—H3···O2*W*^{ii} interactions, with atom C3 acting as hydrogen-bond donor to atom O2*W*$(-x+1, y+\frac{1}{2}, -z+1)$. As a result of the interactions in this substructure, edge-fused $R_8^8(24)$ (Etter, 1990) rings running parallel to [100] are detected (Fig. 2). Additionally, the organic molecules are intertwined through the C2—H2···O2^{iv} interaction; atom C2 acts as hydrogen-bond donor to atom O2$(x-1, y, z+1)$ (see Table 1).

In the second substructure, a channel formed exclusively by water molecules along [100] is observed. Indeed, infinite chains of water molecules, where atoms O2*W* and O1*W* interact through relatively strong hydrogen bonds, are detected. Thus, the structural organization of (I) shows the formation of two intersecting mutually perpendicular columns. The two-dimensional lattices of water molecules lie between layers of 6-methoxyquinoline *N*-oxide molecules. This helps to stabilize and support them in the crystal structure (Fig. 3).

Theoretical calculations of bond lengths and angles were performed by the Hartree–Fock (HF) method with a 6-311++G(d,p) basis set and by density functional theory (DFT) B3LYP, also with a 6-311++G(d,p) basis set, and these values were compared with the experimental values for (I) (Table 2). From these results we can conclude that the DFT basis set 6-311++G(d,p) is better suited in its approach to the experimental data. To enable a better understanding of the properties of (I), we further studied the stability of this

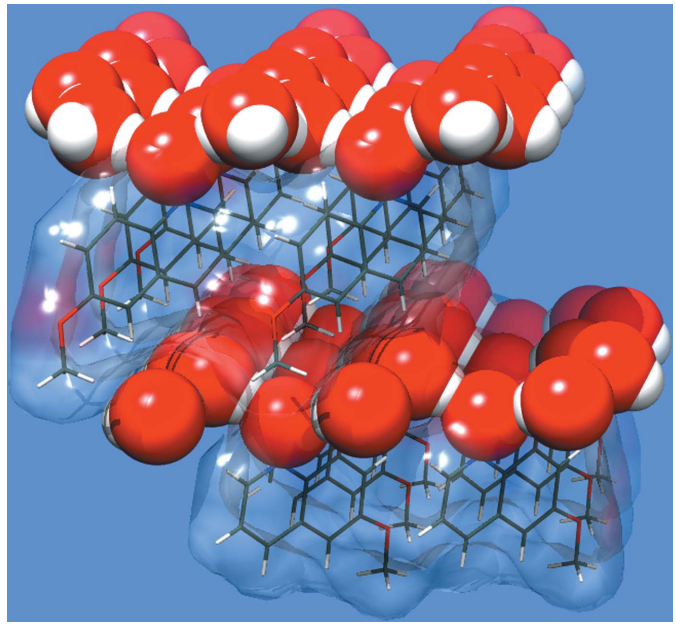

Figure 3
A view of the water channels bridged by O1 atoms to form hydrophilic layers.

compound in the gaseous state, calculating the harmonic frequencies and comparing the results with those observed in the fundamental vibrational frequencies.

The optimized structures, minimum electronic energies and vibrational frequencies were determined using semi-empirical *ab initio* methods and DFT calculations as implemented in the *GAUSSIAN09* program (Frisch *et al.*, 2009).

The frequency calculations of the hydrated complex in the gaseous state were performed from the optimized structure, using HF/6-311++G(d,p) and DFT/6-311++G(d,p) at the B3LYP level of theory, using SCI-PCM (Tomasi *et al.*, 2005) as a model of solvation for both bases. The stability of the compound was checked by the absence of imaginary frequencies in the calculation obtained by both methods. The experimental and simulated IR spectra are shown in Fig. 4. Vibrational analysis of (I) identifies the characteristic bands which correspond to the functional groups that are present in the compound. In the experimental spectrum, the most intense and sharp band is at 1213 cm^{-1} and it can be seen in the simulated spectrum at 1235 cm^{-1}. This signal corresponds to the asymmetric O—N—C stretch. Analogously, one can observe the frequency of axial deformation of the *N*-oxide group at 1279 cm^{-1} and in the simulated spectrum at 1273 cm^{-1}. The axial deformation band of C—O in the methoxy group, which is located at 1016 cm^{-1} in the experimental spectrum and at 1038 cm^{-1} in the simulated one, can also be assigned. These and other experimental and calculated bands are given in Table 3. Comparing the calculated and experimental values allows a good correlation between the bands to be found.

The optimization of the molecular geometry of (I) in the gaseous state was performed in order to analyse the stability of the molecule. The analysis of the total energy and the energy gap between the frontier molecular orbitals HOMO (highest occupied molecular orbital) and LUMO (lowest unoccupied molecular orbital) of the molecule characterize its molecular chemical stability.

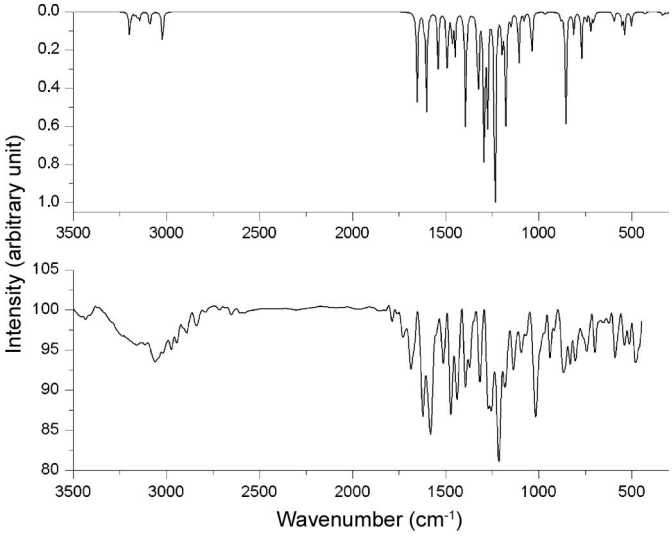

Figure 4
Comparison of the calculated IR spectrum of (I) (top) with the observed spectrum (bottom).

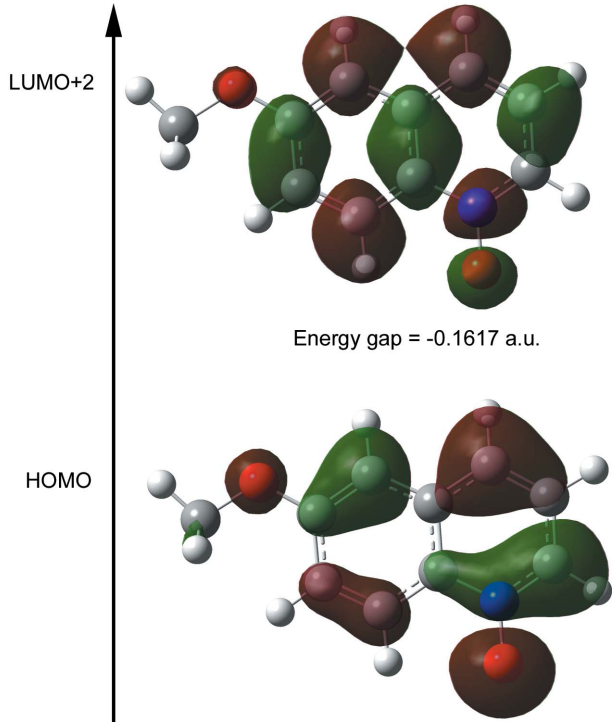

Figure 5
The atomic orbital compositions of the frontier molecular orbital for (I).

Compound (I) shows an absorption band in the UV at λ = 234 nm in acetonitrile. Electronic transitions in this molecular system were analysed using B3LYP/6-311G**(d,p) with SCI-PCM (water) as a model of solvation, yielding the most intense band at λ = 267.93 nm (oscillator strength = 0.2016). This band corresponds to an electronic transition from the HOMO to the third lowest unoccupied molecular orbital, LUMO+2. According to Fig. 5, the HOMO presents a charge density localized over the quinoline ring, and a positive phase is localized over the O atom of the *N*-oxide group. The LUMO is also characterized by a charge distribution over the whole molecule, but that over the O atom of the *N*-oxide group is now negative.

Analysis of the coefficients of the molecular orbitals of the optimized geometry suggests that the HOMO and LUMO+2 orbitals are delocalized over the C—C bonds of the aromatic rings, and therefore the transition involves an electron-density transfer of type $\pi\rightarrow\pi^*$ on the molecular plane of the aromatic backbone. The bathochromic shift of the calculated bands with respect to the experimental bands can be explained by the interaction of the *N*-oxide functional group with the polar solvent (Hsieh *et al.*, 2010).

The Hirshfeld surface provides information not only on the areas of close contact, and therefore of strong interactions, but also on distant contact areas of weak interactions. The structure of (I) has a different environment on each side of the molecule and for this reason the Hirshfeld surface (Fig. 6*b*) is not symmetrical. Each contact on the surface can be identified individually from the colour pattern on the shape index

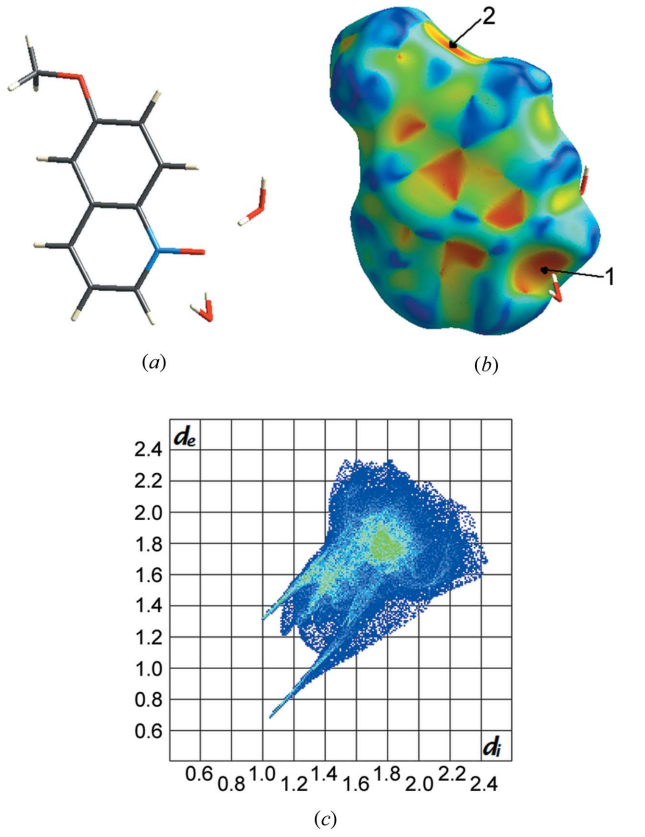

Figure 6
(*a*) Capped-stick drawing of (I) in the orientation used to produce (*b*) the Hirshfeld surface (see *Comment* for colour and labelling information) and (*c*) the two-dimensional fingerprint plot for (I).

surface. The spots (red in the electronic version of the paper) with concave curvature that appear on the surface of the quinoline plane are similar to those occurring on the naphthalene plane (McKinnon *et al.*, 1998). C—H donor regions with convex curvature can be observed, especially around the methyl group (identified by a deep blue colour in Fig. 6*b*). The shorter of the O···H—O contacts between the O atom of the *N*-oxide group and the two water molecules is labelled 1 in Fig. 6(*b*). This concave surface (red) shows clearly the strong interactions on each side of the Hirshfeld surface. Another significant interaction can be seen in Fig. 6(*b*) and is labelled 2. This corresponds to the interaction which links quinoline molecules through the C2—H2···O2($x-1, y, z+1$) contact.

The fingerprint plot analysis of the title structure was performed by comparison with the other related structures, namely 6-methoxy-8-nitroquinoline (Chambers *et al.*, 2004), MQNOHQ (Moreno-Fuquen *et al.*, 2007) and 2,4-dichloro-6-methoxyquinoline (Subashini *et al.*, 2009). The 6-methoxy-8-nitroquinoline and 2,4-dichloro-6-methoxyquinoline systems present fingerprint plots that are more or less symmetrical, as a result of the absence of strong intermolecular interactions. This behaviour is similar to that presented by the naphthalene ring (McKinnon *et al.*, 2004). The two-dimensional fingerprint analysis of MQNOHQ (Moreno-Fuquen *et al.*, 2007), the molecule closest to (I), clearly shows the intermolecular interaction of the O atom of the *N*-oxide group with the O atom of the hydroxy group of the hydroquinone molecule [O···O = 2.6118 (18) Å and O···H = 1.67 (2) Å] through the emergence of an elongated peak projecting towards the bottom of the fingerprint plot. The fingerprint plot analysis of (I) (Fig. 6*c*) reveals the emergence of two sharp peaks, characteristic of the most important hydrogen-bond interactions (O—H···O or C—H···O) that occur between the molecules. The lower peak (where $d_e < d_i$) is more pronounced and corresponds to the interactions O2*W*—H4*W*···O1^{i}, O1*W*—H2*W*···O1^{ii} and C2—H2···O2^{iv}, in which the *N*-oxide molecule plays the role of hydrogen-bond acceptor. Similarly, the upper peak ($d_i < d_e$) corresponds to the C3—H3···O2*W*^{ii} interaction, where (I) acts as a hydrogen-bond donor. This behaviour is reflected in the Hirshfeld surface through the concave surfaces (red), numbered 1 and 2 in Fig. 6(*b*) (see Table 1 for the symmetry codes).

Detailed analysis of the fingerprint plots can evaluate the overlapping contributions from the most important interactions, including O···H, H···H and C···H, facilitating comparison of the surface properties between (I) and MQNOHQ. This analysis shows that the H···H interactions are the largest contributor to the Hirshfeld surfaces for both systems, at 39.2% in MQNOHQ and 47.6% in (I). The contribution of O—H interactions on the surface is similar for both systems [11.8% in (I) and 12.8% in MQNOHQ]. The H···O distances for the O2*W*—H4*W*···O1^{i} and O1*W*—H2*W*···O1^{ii} interactions in (I) [1.87 (3) and 1.92 (3) Å, respectively] are more elongated than that observed in MQNOHQ (1.67 Å), probably because they also participate in the formation of the water channels along [001].

In conclusion, the O—H···O and C—H···O hydrogen-bond interactions in (I) are involved in the construction of the supramolecular architecture, and the water molecules play a major role in the formation of channels along [100] and [001]. The formation of the water channels between the layers of *N*-oxide molecules gives greater stability to the crystal structure. The IR spectrum of (I) computed at the DFT level with basis set 6-311++G(d,p) reproduces the vibrational wavenumbers and intensities with an accuracy which allows reliable vibrational assignments. Finally, analysis of the Hirshfeld surface and fingerprint plot for (I) allow the visualization of O···H—O hydrogen bonds as close intermolecular contacts within the supramolecular crystal lattice.

Experimental

The reagent was purchased from Aldrich Chemical Co. It was recrystallized from acetonitrile to give (I), which melted at 376 (1) K.

Crystal data

$C_{10}H_9NO_2\cdot 2H_2O$
$M_r = 211.21$
Monoclinic, $P2_1$
$a = 5.0000$ (2) Å
$b = 17.1211$ (6) Å
$c = 6.4421$ (3) Å
$\beta = 105.864$ (4)°
$V = 530.48$ (4) Å^3
$Z = 2$
Mo $K\alpha$ radiation
$\mu = 0.10$ mm^{-1}
$T = 123$ K
0.21 × 0.16 × 0.12 mm

Table 1
Hydrogen-bond geometry (Å, °).

D—H···A	D—H	H···A	D···A	D—H···A
O2W—H4W···O1^{i}	0.85 (3)	1.87 (3)	2.721 (2)	179 (3)
O1W—H2W···O1^{ii}	0.86 (3)	1.92 (3)	2.774 (2)	178 (2)
O1W—H1W···O2W^{ii}	0.82 (3)	2.00 (3)	2.817 (2)	170 (2)
O2W—H3W···O1W^{iii}	0.86 (3)	1.96 (3)	2.828 (2)	177 (2)
C3—H3···O2W^{ii}	0.95	2.45	3.375 (2)	164
C2—H2···O2^{iv}	0.95	2.46	3.404 (2)	176

Symmetry codes: (i) $x, y, z-1$; (ii) $-x+1, y+\frac{1}{2}, -z+1$; (iii) $-x+2, y-\frac{1}{2}, -z+1$; (iv) $x-1, y, z+1$.

Table 2
Comparison of selected geometric data for (I) (Å, °) from X-ray and calculated (HF and DFT) data.

Bond lengths	X-ray	HF/6–311++G(d,p)	DFT/B3LYP/ 6–311++G(d,p)
O1—N1	1.338 (2)	1.2983	1.2934
O2—C8	1.372 (2)	1.3425	1.3594
O2—C10	1.434 (2)	1.41	1.4319
N1—C1	1.343 (2)	1.3022	1.3445
N1—C5	1.401 (3)	1.3819	1.4031
Bond angles			
C8—O2—C10	116.89 (15)	120.4905	119.1327
O1—N1—C5	118.10 (15)	118.9222	119.5823
O1—N1—C1	119.62 (15)	120.6939	120.986
C1—N1—C5	122.26 (17)	120.3839	119.4317

Data collection

Oxford Gemini S diffractometer
Absorption correction: multi-scan (*CrysAlis PRO*, Oxford Diffraction, 2010)
T_{min} = 0.965, T_{max} = 1.000
2836 measured reflections
1928 independent reflections
1760 reflections with $I > 2\sigma(I)$
R_{int} = 0.017

Refinement

$R[F^2 > 2\sigma(F^2)]$ = 0.035
$wR(F^2)$ = 0.079
S = 1.05
1928 reflections
153 parameters
1 restraint
H atoms treated by a mixture of independent and constrained refinement
$\Delta\rho_{max}$ = 0.15 e Å^{-3}
$\Delta\rho_{min}$ = −0.15 e Å^{-3}

C-bound H atoms were positioned geometrically, with C—H = 0.95 Å for aromatic H atoms or 0.98 Å for methyl H atoms, and refined using a riding model, with U_{iso}(H) = 1.2U_{eq}(C) for aromatic H atoms or 1.5U_{eq}(C) for methyl H atoms. Water atoms were located in a difference Fourier map and were refined freely.

Data collection: *CrysAlis PRO* (Oxford Diffraction, 2010); cell refinement: *CrysAlis PRO*; data reduction: *CrysAlis PRO*; program(s) used to solve structure: *SHELXS97* (Sheldrick, 2008); program(s) used to refine structure: *SHELXL97* (Sheldrick, 2008); molecular graphics: *ORTEP-3 for Windows* (Farrugia, 2012) and *Mercury* (Macrae *et al.*, 2008); software used to prepare material for publication: *WinGX* (Farrugia, 2012).

RMF is grateful to the Spanish Research Council (CSIC) for the use of a free-of-charge licence to the Cambridge Structural Database (Allen, 2002). RMF also thanks the Universidad del Valle, Colombia, for partial financial support.

Table 3
Comparison of the observed and calculated vibrational frequences (cm^{-1}) for (I).

Assignment	Observed	Calculated
C—N out of plane bending (wagging)	851	769
C—O vibrational axial deformation of methoxy group	1016	1038
C—O—C asymmetric stretching of methoxy group	1135	1176
O—N—C asymmetric stretching	1213	1235
N—O vibrational axial deformation of *N*-oxide group	1279	1293
C—N—C symmetric stretching	1392	1392
C—O—C asymmetric stretching	1511	1490
C—C symmetric stretching in aromatic rings	1685	1653
C—H symmetric stretching at methyl group	3061	3021
C—H asymmetric stretching at methyl group		3090
C—H vibrational axial deformation at aromatic rings		3197

Supplementary data for this paper are available from the IUCr electronic archives (Reference: TP3021). Services for accessing these data are described at the back of the journal.

References

Allen, F. H. (2002). *Acta Cryst.* B**58**, 380–388.
Allen, F. H., Kennard, O., Watson, D. G., Brammer, L., Orpen, A. G. & Taylor, R. (1987). *J. Chem. Soc. Perkin Trans. 2*, pp. S1–S19.
Ballabio, M., Sbraletta, P., Mantegani, S. & Brambilla, E. (1992). *Tetrahedron*, **48**, 4555–4566.
Biavatti, M. W., Vieira, P. C., da Silva, M. F. G. F., Fernandes, J. B., Victor, S. R., Pagnocca, F. C., Albuquerque, S., Caracelli, I. & Zukerman-Schpector, J. (2002). *J. Braz. Chem. Soc.* **13**, 66–70.
Campbell, S. F., Hardstone, J. D. & Palmer, M. J. (1988). *J. Med. Chem.* **31**, 1031–1035.
Chambers, R. D., Holling, D., Sandford, G., Batsanov, A. S. & Howard, J. A. K. (2004). *J. Fluorine Chem.* **125**, 661–671.
Cukierman, S. (2000). *Biophys. J.* **78**, 1825–1834.
Desiraju, G. R. (1989). *Crystal Engineering: The Design of Organic Solids*. Amsterdam: Elsevier.
Desiraju, G. R. (1996). *Acc. Chem. Res.* **29**, 441–449.
Etter, M. (1990). *Acc. Chem. Res.* **23**, 120–126.
Farrugia, L. J. (2012). *J. Appl. Cryst.* **45**, 849–854.
Frisch, M. J., *et al.* (2009). *GAUSSIAN09*. Gaussian Inc., Wallingford, Connecticut, USA.
Hsieh, C.-P., Lu, H.-P., Chiu, C.-L., Lee, C.-W., Chuang, S.-H., Mai, C.-L., Yen, W.-N., Hsu, S.-J., Diau, E. W.-G. & Yeh, C.-Y. (2010). *J. Mater. Chem.* **20**, 1127–1134.
Jude, K. M., Wright, S. K., Tu, C., Silverman, D. N., Viola, R. E. & Christianson, D. W. (2002). *Biochemistry*, **41**, 2485–2491.
Kaiser, J. P., Feng, Y. & Bollag, J. M. (1996). *Microbiol. Rev.* **60**, 483–498.
Katakura, R. & Koide, Y. (2006). *Inorg. Chem.* **45**, 5730–5732.
Leiserowitz, L. & Weinstein, M. (1975). *Acta Cryst.* B**31**, 1463–1466.
Macrae, C. F., Bruno, I. J., Chisholm, J. A., Edgington, P. R., McCabe, P., Pidcock, E., Rodriguez-Monge, L., Taylor, R., van de Streek, J. & Wood, P. A. (2008). *J. Appl. Cryst.* **41**, 466–470.
McKinnon, J. J., Mitchell, A. S. & Spackman, M. A. (1998). *Chem. Commun.* pp. 2071–2072.
McKinnon, J. J., Spackman, M. A. & Mitchell, A. S. (2004). *Acta Cryst.* B**60**, 627–668.
Moreno-Fuquen, R., Shankland, K. & Fabbiani, F. P. A. (2007). *Acta Cryst.* E**63**, o2891.
Moreno-Fuquen, R., Valencia, L., Kennedy, A. R., Gilmour, D. & Ribeiro, L. (2010). *Z. Kristallogr.* **225**, 396–400.
Nardelli, M. (1995). *J. Appl. Cryst.* **28**, 659.
Oxford Diffraction (2010). *CrysAlis PRO*. Oxford Diffraction Ltd, Yarnton, England.

Polshettiwar, V. & Varma, R. S. (2008). *Pure Appl. Chem.* **80**, 777–790.
Sakamoto, M. (2004). *Enantiomer Separation. Fundamentals and Practical Methods*, edited by F. Toda, pp. 104–105. Dordrecht: Kluwer Academic Publishers.
Sheldrick, G. M. (2008). *Acta Cryst.* A**64**, 112–122.
Somvanshi, R. K., Subashini, R., Dhanasekaran, V., Arulprakash, G., Das, S. N. & Dey, S. (2008). *J. Chem. Crystallogr.* **38**, 381–386.
Subashini, R., Hathwar, V. R., Manivel, P., Prabakaran, K. & Khan, F. N. (2009). *Acta Cryst.* E**65**, o370.
Sui, Z., Altom, J., Nguyen, V. N., Fernandez, J., Bernstein, J. I., Hilliard, J. J., Barrett, J. F., Podlogar, B. L. & Ohemeng, K. A. (1998). *Bioorg. Med. Chem.* **6**, 735–742.
Tieleman, D. P., Biggin, P. C., Smith, G. R. & Sansom, M. S. (2001). *Q. Rev. Biophys.* **34**, 473–561.
Tomasi, J., Mennucci, B. & Cammi, R. (2005). *Chem. Rev.* **105**, 2999–3093.
Towers, G. H. N., Graham, E. A., Spenser, I. D. & Abramowski, Z. (1981). *Planta Med.* **41**, 136–142.

supplementary materials

Acta Cryst. (2013). C**69**, 665-670 [doi:10.1107/S0108270113011979]

Supramolecular study, Hirshfeld analysis and theoretical study of 6-methoxyquinoline *N*-oxide dihydrate

Rodolfo Moreno-Fuquen, Geraldine Hernandez, Alan R. Kennedy and Catriona A. Morrison

6-Ethoxyquinoline N-oxide dihydrate

Crystal data

$C_{10}H_9NO_2{\cdot}2H_2O$
$M_r = 211.21$
Monoclinic, $P2_1$
Hall symbol: P 2yb
$a = 5.0000\ (2)$ Å
$b = 17.1211\ (6)$ Å
$c = 6.4421\ (3)$ Å
$\beta = 105.864\ (4)°$
$V = 530.48\ (4)$ Å^3
$Z = 2$
$F(000) = 224$
$D_x = 1.322$ Mg m^{-3}
Melting point: 386(1) K
Mo $K\alpha$ radiation, $\lambda = 0.71073$ Å
Cell parameters from 2837 reflections
$\theta = 3.5–26.0°$
$\mu = 0.10$ mm^{-1}
$T = 123$ K
Prism, pale yellow
0.21 × 0.16 × 0.12 mm

Data collection

Oxford Gemini S diffractometer
Radiation source: fine-focus sealed tube
Graphite monochromator
ω scans
Absorption correction: multi-scan (*CrysAlis PRO*, Oxford Diffraction, 2009)
$T_{min} = 0.965$, $T_{max} = 1.000$
2836 measured reflections
1928 independent reflections
1760 reflections with $I > 2\sigma(I)$
$R_{int} = 0.017$
$\theta_{max} = 26.0°$, $\theta_{min} = 3.5°$
$h = -6\rightarrow6$
$k = -20\rightarrow21$
$l = -7\rightarrow7$

Refinement

Refinement on F^2
Least-squares matrix: full
$R[F^2 > 2\sigma(F^2)] = 0.035$
$wR(F^2) = 0.079$
$S = 1.05$
1928 reflections
153 parameters
1 restraint
Primary atom site location: structure-invariant direct methods
Secondary atom site location: difference Fourier map
Hydrogen site location: inferred from neighbouring sites
H atoms treated by a mixture of independent and constrained refinement
$w = 1/[\sigma^2(F_o^2) + (0.0363P)^2 + 0.0351P]$ where $P = (F_o^2 + 2F_c^2)/3$
$(\Delta/\sigma)_{max} < 0.001$
$\Delta\rho_{max} = 0.15$ e Å^{-3}
$\Delta\rho_{min} = -0.15$ e Å^{-3}

Special details

Geometry. All e.s.d.'s (except the e.s.d. in the dihedral angle between two l.s. planes) are estimated using the full covariance matrix. The cell e.s.d.'s are taken into account individually in the estimation of e.s.d.'s in distances, angles and torsion angles; correlations between e.s.d.'s in cell parameters are only used when they are defined by crystal symmetry. An approximate (isotropic) treatment of cell e.s.d.'s is used for estimating e.s.d.'s involving l.s. planes.

Refinement. Refinement of F^2 against ALL reflections. The weighted *R*-factor *wR* and goodness of fit *S* are based on F^2, conventional *R*-factors *R* are based on *F*, with *F* set to zero for negative F^2. The threshold expression of $F^2 > \sigma(F^2)$ is used only for calculating *R*-factors(gt) *etc*. and is not relevant to the choice of reflections for refinement. *R*-factors based on F^2 are statistically about twice as large as those based on *F*, and *R*-factors based on ALL data will be even larger.

Fractional atomic coordinates and isotropic or equivalent isotropic displacement parameters (Å²)

	x	*y*	*z*	U_{iso}*/U_{eq}
O1	0.5089 (3)	0.79875 (8)	0.7368 (2)	0.0280 (4)
O2	1.0341 (3)	1.06063 (8)	0.2866 (2)	0.0269 (4)
O1W	0.7678 (3)	1.25800 (10)	0.6839 (3)	0.0335 (4)
O2W	0.6638 (3)	0.72504 (9)	0.1254 (3)	0.0268 (3)
N1	0.5114 (3)	0.87590 (9)	0.7698 (3)	0.0208 (4)
C1	0.3832 (4)	0.90549 (12)	0.9102 (3)	0.0239 (5)
H1	0.2954	0.8715	0.9880	0.029*
C2	0.3784 (4)	0.98627 (12)	0.9423 (3)	0.0248 (5)
H2	0.2899	1.0068	1.0436	0.030*
C3	0.5005 (4)	1.03582 (12)	0.8289 (3)	0.0224 (4)
H3	0.4942	1.0906	0.8499	0.027*
C4	0.6376 (4)	1.00521 (11)	0.6787 (3)	0.0192 (4)
C5	0.6453 (4)	0.92332 (11)	0.6517 (3)	0.0202 (4)
C6	0.7859 (4)	0.89034 (12)	0.5088 (3)	0.0209 (4)
H6	0.7933	0.8353	0.4934	0.025*
C7	0.9110 (4)	0.93845 (12)	0.3931 (3)	0.0219 (5)
H7	1.0063	0.9163	0.2984	0.026*
C8	0.8998 (4)	1.02078 (11)	0.4132 (3)	0.0204 (5)
C9	0.7674 (4)	1.05362 (12)	0.5544 (3)	0.0215 (4)
H9	0.7629	1.1088	0.5687	0.026*
C10	1.0346 (5)	1.14424 (12)	0.3004 (4)	0.0356 (6)
H10A	1.1272	1.1603	0.4487	0.053*
H10B	0.8426	1.1634	0.2598	0.053*
H10C	1.1343	1.1661	0.2023	0.053*
H1W	0.634 (5)	1.2537 (14)	0.734 (4)	0.037 (7)*
H2W	0.679 (5)	1.2708 (15)	0.555 (4)	0.041 (8)*
H3W	0.838 (6)	0.7354 (14)	0.180 (4)	0.037 (7)*
H4W	0.616 (6)	0.7473 (18)	0.003 (5)	0.060 (9)*

Atomic displacement parameters (Å²)

	U^{11}	U^{22}	U^{33}	U^{12}	U^{13}	U^{23}
O1	0.0431 (9)	0.0177 (7)	0.0231 (8)	−0.0011 (6)	0.0089 (7)	−0.0008 (6)
O2	0.0337 (8)	0.0249 (8)	0.0258 (8)	−0.0023 (6)	0.0144 (7)	0.0018 (7)
O1W	0.0269 (9)	0.0466 (10)	0.0286 (9)	0.0045 (7)	0.0101 (8)	0.0107 (8)
O2W	0.0293 (9)	0.0277 (8)	0.0245 (8)	−0.0015 (6)	0.0095 (7)	0.0032 (7)
N1	0.0230 (9)	0.0196 (9)	0.0183 (9)	0.0009 (6)	0.0033 (7)	−0.0003 (7)

C1	0.0250 (11)	0.0297 (12)	0.0173 (11)	−0.0008 (8)	0.0062 (9)	0.0004 (9)
C2	0.0226 (11)	0.0341 (13)	0.0188 (11)	0.0067 (8)	0.0072 (8)	−0.0051 (9)
C3	0.0235 (11)	0.0216 (10)	0.0214 (11)	0.0034 (8)	0.0049 (9)	−0.0038 (8)
C4	0.0165 (10)	0.0208 (10)	0.0190 (10)	0.0028 (8)	0.0028 (8)	−0.0002 (9)
C5	0.0185 (10)	0.0223 (10)	0.0180 (11)	0.0004 (8)	0.0019 (9)	0.0001 (8)
C6	0.0216 (11)	0.0207 (10)	0.0187 (10)	0.0024 (8)	0.0024 (8)	−0.0042 (9)
C7	0.0206 (11)	0.0280 (12)	0.0177 (11)	0.0017 (8)	0.0064 (9)	−0.0041 (9)
C8	0.0158 (10)	0.0252 (12)	0.0190 (11)	−0.0004 (7)	0.0027 (8)	0.0008 (8)
C9	0.0225 (10)	0.0190 (10)	0.0220 (11)	0.0022 (8)	0.0042 (8)	−0.0012 (9)
C10	0.0478 (15)	0.0255 (12)	0.0396 (14)	−0.0049 (10)	0.0225 (12)	0.0045 (11)

Geometric parameters (Å, º)

O1—N1	1.338 (2)	C3—H3	0.9500
O2—C8	1.372 (2)	C4—C5	1.415 (3)
O2—C10	1.434 (2)	C4—C9	1.426 (3)
O1W—H1W	0.82 (3)	C5—C6	1.420 (3)
O1W—H2W	0.86 (3)	C6—C7	1.371 (3)
O2W—H3W	0.86 (3)	C6—H6	0.9500
O2W—H4W	0.85 (3)	C7—C8	1.418 (3)
N1—C1	1.343 (2)	C7—H7	0.9500
N1—C5	1.401 (3)	C8—C9	1.382 (3)
C1—C2	1.400 (3)	C9—H9	0.9500
C1—H1	0.9500	C10—H10A	0.9800
C2—C3	1.368 (3)	C10—H10B	0.9800
C2—H2	0.9500	C10—H10C	0.9800
C3—C4	1.429 (3)		
C8—O2—C10	116.89 (15)	C4—C5—C6	120.58 (17)
H1W—O1W—H2W	98 (2)	C7—C6—C5	119.61 (19)
H3W—O2W—H4W	106 (2)	C7—C6—H6	120.2
O1—N1—C1	119.62 (15)	C5—C6—H6	120.2
O1—N1—C5	118.10 (15)	C6—C7—C8	120.82 (18)
C1—N1—C5	122.26 (17)	C6—C7—H7	119.6
N1—C1—C2	120.20 (18)	C8—C7—H7	119.6
N1—C1—H1	119.9	O2—C8—C9	126.11 (18)
C2—C1—H1	119.9	O2—C8—C7	113.72 (16)
C3—C2—C1	120.39 (18)	C9—C8—C7	120.15 (18)
C3—C2—H2	119.8	C8—C9—C4	120.43 (18)
C1—C2—H2	119.8	C8—C9—H9	119.8
C2—C3—C4	120.06 (18)	C4—C9—H9	119.8
C2—C3—H3	120.0	O2—C10—H10A	109.5
C4—C3—H3	120.0	O2—C10—H10B	109.5
C5—C4—C9	118.37 (16)	H10A—C10—H10B	109.5
C5—C4—C3	118.73 (17)	O2—C10—H10C	109.5
C9—C4—C3	122.90 (17)	H10A—C10—H10C	109.5
N1—C5—C4	118.34 (16)	H10B—C10—H10C	109.5
N1—C5—C6	121.08 (17)		
O1—N1—C1—C2	−178.45 (17)	C3—C4—C5—C6	−178.23 (18)

C5—N1—C1—C2	0.3 (3)	N1—C5—C6—C7	178.96 (18)
N1—C1—C2—C3	1.0 (3)	C4—C5—C6—C7	−1.2 (3)
C1—C2—C3—C4	−0.9 (3)	C5—C6—C7—C8	−0.5 (3)
C2—C3—C4—C5	−0.4 (3)	C10—O2—C8—C9	−0.7 (3)
C2—C3—C4—C9	179.60 (18)	C10—O2—C8—C7	−179.23 (17)
O1—N1—C5—C4	177.15 (16)	C6—C7—C8—O2	−179.82 (17)
C1—N1—C5—C4	−1.7 (3)	C6—C7—C8—C9	1.5 (3)
O1—N1—C5—C6	−3.0 (3)	O2—C8—C9—C4	−179.36 (18)
C1—N1—C5—C6	178.22 (17)	C7—C8—C9—C4	−0.9 (3)
C9—C4—C5—N1	−178.36 (17)	C5—C4—C9—C8	−0.7 (3)
C3—C4—C5—N1	1.6 (3)	C3—C4—C9—C8	179.27 (18)
C9—C4—C5—C6	1.8 (3)		

Hydrogen-bond geometry (Å, º)

D—H···*A*	*D*—H	H···*A*	*D*···*A*	*D*—H···*A*
O2*W*—H4*W*···O1^{i}	0.85 (3)	1.87 (3)	2.721 (2)	179 (3)
O1*W*—H2*W*···O1^{ii}	0.86 (3)	1.92 (3)	2.774 (2)	178 (2)
O1*W*—H1*W*···O2*W*^{ii}	0.82 (3)	2.00 (3)	2.817 (2)	170 (2)
C3—H3···O2*W*^{ii}	0.95	2.45	3.375 (2)	164
O2*W*—H3*W*···O1*W*^{iii}	0.86 (3)	1.96 (3)	2.828 (2)	177 (2)
C2—H2···O2^{iv}	0.95	2.46	3.404 (2)	176

Symmetry codes: (i) *x*, *y*, *z*−1; (ii) −*x*+1, *y*+1/2, −*z*+1; (iii) −*x*+2, *y*−1/2, −*z*+1; (iv) *x*−1, *y*, *z*+1.

Comparison of selected geometric data for (I) (Å, °) from calculated (DFT) and X-ray data

Bond lengths	X-ray	HF/6-311++G(d,p)	B3LYP/6-311++G(d,p)
O1—N1	1.338 (2)	1.2983	1.2934
O2—C5	1.372 (2)	1.3425	1.3594
O2—C10	1.434 (2)	1.41	1.4319
N1—C1	1.343 (2)	1.3022	1.3445
N1—C8	1.401 (3)	1.3819	1.4031
Bond angles			
C5—O2—C10	116.89 (15)	120.4905	119.1327
O1—N1—C8	118.10 (15)	118.9222	119.5823
O1—N1—C1	119.62 (15)	120.6939	120.986
C1—N1—C8	122.26 (17)	120.3839	119.4317

Comparison of the observed and calculated vibrational frequences (cm^{-1}) for (I)

Assignment	Observed	Calculated
C—N out of plane bending (wagging)	851	769
C—O vibrational axial deformation of methoxy group	1016	1038
C—O—C asymmetric stretching of mhethoxy group	1135	1176
O—N—C asymmetric stretching	1213	1235
N—O vibrational axial deformation of N-oxide group	1279	1293

C—N—C symmetric stretching	1392	1392
C—O—C asymmetric stretching	1511	1490
C—C symmetric stretching in the aromatic rings	1685	1653
C—H symmetric stretching at methyl group	3061	3021
C—H asymmetric stretching at methyl group		3090
C—H vibrational axial deformation at aromatic rings		3197